Electronic Supplementary Information

Synergistical Transition Metal Ion Co-Doping and Multiple Functional Additive Passivation for Realizing 25.30% Efficiency Perovskite Solar Cells

Yuting Chen [‡a], Qi Wang [‡a], Yuqi Yao [a], Jiewei Yang [a], Weijian Tang [a], Wuke Qiu [a], Yihui Wu *[ab], and Qiang Peng *[ab]

[a]School of Chemical Engineering and State Key Laboratory of Polymer Materials Engineering, Sichuan University, Chengdu 610065, China. E-mails: yihuiwu@scu.edu.cn; qiangpeng@scu.edu.cn

[b]Engineering Research Center of Alternative Energy Materials & Devices, Ministry of Education, Sichuan University, Chengdu 610065, China

[‡]These authors contributed equally to this work.

Experimental Procedures

Materials: All the chemicals were used as received. Lead iodide (≥98%) and Formamidinium iodide (FAI) were purchased from Advanced Election Technology, Co. Ltd. $SnCl_2 \cdot 2H_2O$ (>99.99%), 4,4'-dithiodibutyric acid (DDA, >95%), and anisole were purchased from Aladdin. $NbCl_5$ (99.999%), $TaCl_5$ (99.995%), RbI (99.9%), thioglycolic acid (TGA, 98%), urea, lithium Bis(trifluoromethanesulfonyl)imide salt (Li-TFSI) and 4-tert-butylpyridine (tBP) were purchased from Sigma-Aldrich. CsCl (99.999%) was purchased from Alfa-aesar. Cobalt(III) Tris(bis(trifluoromethylsulfonyl)imide)) salt (Co(III) TFSI, FK209) were purchased from Greatcell solar. Methylammonium iodide (MAI) and spiro-OMeTAD were purchased from Xi'an p-oled. Dimethylformamide (DMF), dimethyl sulfoxide (DMSO), chlorobenzene (CB), isopropyl alcohol (IPA) and acetonitrile were purchased from Sigma-Aldrich and used without purification.

Device fabrication

Preparation of SnO_2 ETLs:

The pristine compact SnO_2 layer was fabricated on the cleaned and patterned FTO substrates (AGC22-8A, Advanced Election Technology, Co. Ltd.) using a chemical bath deposition (CBD) method. Briefly, 625 mg of urea and 137.5 mg of $SnCl_2 \cdot 2H_2O$ were dissolved in 50 mL of ultrapure water. Then, 625 μL of HCl and 12.5 μL of TGA were added into this solution. The obtained CBD solution was loaded onto a glass reaction vessel. The cleaned FTO substrate were vertically placed into the vessel and the reaction was kept at 90 °C for 5.5 h. After the reaction is completed, the FTO/SnO_2 substrate was removed from the reaction vessel and cleaned *via* sonication with deionized water and IPA for 5 min each. The FTO/SnO_2 substrate was then annealed in an ambient environment at 170 °C for 60 min. After cooling down to room temperature, a 10 mM of KCl aqueous solution was spin-coated onto the FTO/SnO_2 substrates and annealed at 100 °C for 10 min. For the doped SnO_2 film, 5 mol.% $NbCl_5$, or 5 mol.% $TaCl_5$, or 2.5 mol.% $NbCl_5$ and 2.5 mol.% $TaCl_5$ were added directly with the $SnCl_2 \cdot 2H_2O$ into the ultrapure water. The other fabrication procedures were identical to the that of the pristine SnO_2.

Deposition of RbCsFAMA quadruple-cation perovskite films:

For the RbCsFAMA based perovskite films, the perovskite solution was prepared by mixing 645.4 mg of PbI_2, 216.7 mg of FAI, 11.1 mg of MAI, 11.8 mg of CsCl and 8.9 mg of RbI in a mixed solvent (DMF:DMSO = 4:1, v/v). The solution was stirred for 12 h. After that, the perovskite ink

was deposited on the above mentioned FTO/SnO_2 substrates *via* spin coating at 1000 rpm for 10 second with a ramp of 200, and 4000 rpm for 30 second (2000 rpm ramp). For 20 seconds into the second step, 110 μL of anisole was deposited onto the substrate. Then the wet film was annealed at 110 ^oC for 60 min. After the perovskite film was cooled down to room temperature, a 5 mg/mL of PEAI/IPA solution was spin-coated at 5000 rpm for 30 s and no annealing was required.

Deposition of CsFAMA triple-cation perovskite films:

For the triple cation PSCs, the precursor solution was prepared by mixing 677.3 mg of PbI_2, 240.2 mg of FAI, 19.5 mg of CsI, 11.3 mg of $PbBr_2$, 3.2 mg of MABr in a mixed solvent (DMF:DMSO = 4:1,v/v), 5 mol% of excess PbI_2 was needed to improve the device performance. Then, 15 mol% MACl was added to the perovskite precursor solution and stirred for 2h. After that, 30 μL perovskite solution was deposited on FTO/SnO_2 substrate *via* spin-coating at 1000 rpm for 10 s, subsequently at 5000 rpm for 40 s. 110 μL anisole was slowly dropped onto the center of film at 12 seconds before the end of spin-coating. The wet film was annealed at 110 ^oC for 20 min. After the perovskite film was cooled down to room temperature, a 5 mg/mL of PEAI/IPA solution was spin-coated at 5000 rpm for 30 s and no annealing was required.

Deposition of CsFA double-cation perovskite films:

For the MA-free, Cs/FA perovskite, the precursor solution was comprised of 52 mg of CsI, 186 mg of FAI, 8 mg of FABr, 591 mg of PbI_2, 18.6 mg of $PbCl_2$ in 1 mL of DMF and DMSO (4:1, v/v). The precursor solution was deposited on compact SnO_2 substrate by a consecutive two-step spin-coating process at 1000 and 4000 rpm for 10 and 40 s, respectively. 110 μL of anisole was dropped onto the substrate at 20 s before the end. And then the wet film was annealed at 110 ^oC for 20 min. After the perovskite film was cooled down to room temperature, a 5 mg/mL of PEAI/IPA solution was spin-coated at 5000 rpm for 30 s and no annealing was required.

Regulation of perovskite film with functional molecule:

For the regulation of perovskite film, a certain amount of DDA was added directly to the perovskite precursor solution (DMF:DMSO = 4:1). The concentration of DDA was 0.01 mg/mL, which was optimized on the basis of the influence on the device performance. Other film fabrication procedures were the same as the above.

Fabrication of HTL and electrode:

When the perovskite films were cooled to room temperature, a solution of spiro-OMeTAD/CB (100 mg mL^{-1}) was spin coated onto perovskite films at 4000 rpm for 30 s in glove box, where 40

μL 4-tert-butylpyridine, 24.5 μL Li-TFSI/acetonitrile (520 mg mL^{-1}) and 49 μL Co-TFSI/acetonitrile (300 mg mL^{-1}) were used as the additives. Finally, 8 nm of MoO_3 and 120 nm of Ag electrode were deposited by thermal evaporation. After deposition of metal electrode, all devices were stored in a desiccator overnight and then the *J-V* curves were measured.

Characterization

The top-view and the cross-sectional SEM images were obtained by using a Titachi S4800 field-emission scanning electron microscopy (Hitachi High Technologies Corporation).

AFM was recorded from Bruker Innova atomic microscopy.

The UV-visible absorption spectra of the solution and thin films were measured from the absorbance model (without integrating sphere) using PerkinElmer Lambda 950 UV−vis spectrophotometer with a scanning rate of 600 nm/min in the range of 900-300 nm at a step bandwidth of 1 nm. The type of baseline calibration was the 100% transmittance baseline.

The XRD patterns of the perovskite films were recorded on Bruker D8 advance with a Cu Kα radiation (40 kV, 40 mA) and a scanning rate of 5°/ min in the 2θ range of 5-50° at a step size of 0.02 s.

The steady PL spectra and time-resolved PL decay measurements were performed using an FLS980 Series of Fluorescence Spectrometers. For the PL measurement, the excitation source was a monochromatized Xe lamp (peak wavelength at 500 nm with a line width of 2 nm). For TRPL, the excitation source was a supercontinuum pulsed laser sources (YSL SC-PRO) with an excitation wavelength at 800 nm and a repetition rate of 0.1 MHz.

Monochromatic external quantum efficiency (EQE) spectra were recorded as functions of wavelength with a monochromatic incident light of 1 x 10^{16} photons cm^{-2} in alternating current mode with a bias voltage of 0 V (QE-R3011). The light intensity of the solar simulator was calibrated by a standard silicon solar cell provided by PV Measurements.

Electrochemical impedance spectroscopy (EIS) was obtained by using a potentiometer (CHI604E, CH instrument) under dark conditions in the frequency range from 1 MHz to 10 mHz with an AC amplitude of 5 mV.

Mott-Schottky analysis were conducted by using a potentiometer (CHI604E, CH instrument) at the frequency of 1000 Hz in the applied voltage range from 0 V to 1.5 V with an AC amplitude of 5 mV.

A Fourier transform infrared spectroscopy (FT-IR, Thermo Fisher Nicolet Is5) was used to collect the FT-IR spectral data for the samples.

The liquid state ^{1}H nuclear magnetic resonance (NMR) measurements were recorded on JNM-ECZ400S/L1 spectrometer (TMS as an internal standard ($\delta = 0$)).

Contact angles were measured using a KRüSS DSA30 drop shape analyzer with perovskite solution as testing liquids.

UPS and XPS spectra were recorded by a Thermo-Fisher ESCALAB Xi+ system. For XPS measurement, radiation was produced by a monochromatic 75 W Al Kα excitation centred at 1486.7 eV. For UPS measurement, He I ultraviolet radiation source of 21.22 eV was used.

The current-voltage characteristics were measured by Keithley 2400 source and the solar simulator with standard AM 1.5G (100 mW/cm^2, SAN EI: Japan) under ambient conditions. The *J-V* curves were measured by forward (-0.1 V to 1.5 V forward bias) or reverse (1.5 V to -0.1 V) scans with a delay time of 100 ms for each point. The *J-V* curves for all devices were obtained by masking the cells with a metal mask 0.09 cm^2 in area.

The devices for long-term stability measurement were stored in a N_2-filled glovebox. After various periods of time, the *J-V* measurements were performed.

The dynamic MPP tracking was carried out in a home-made N_2-filled box under 1 sun continuous illumination (white light LED array) with temperature of ~30 °C. The MPP was automatically recalculated every 2 h by tracking the *J-V* curve.

Results and Discussion

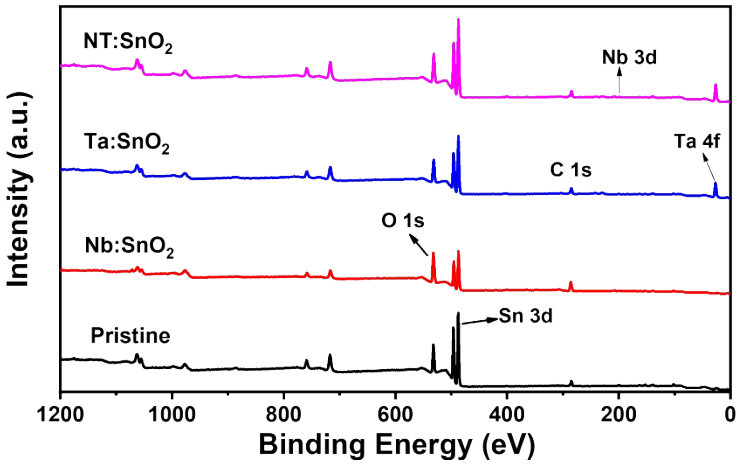

Fig. S1. The survey of XPS spectra for the pristine and doped SnO_2 films.

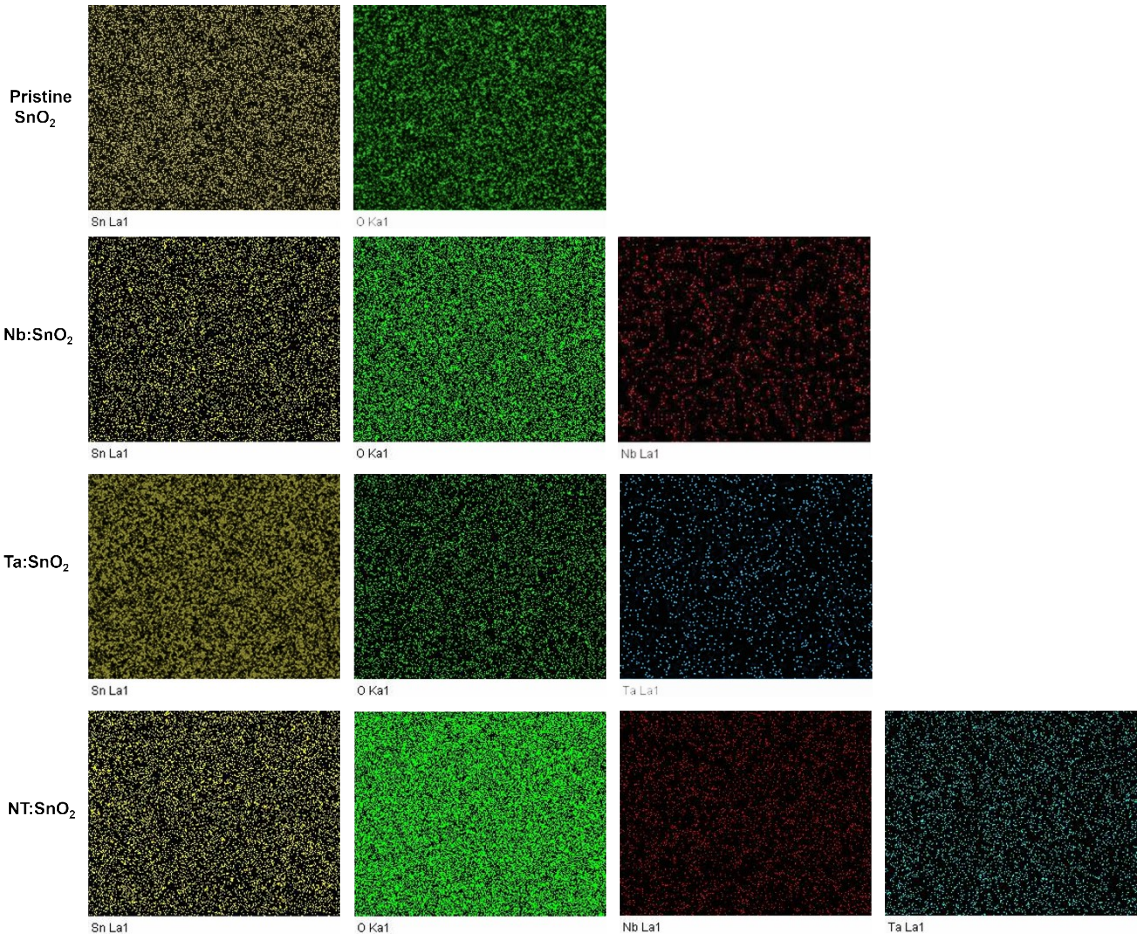

Fig. S2. EDS mapping for the pristine and doped SnO_2 films.

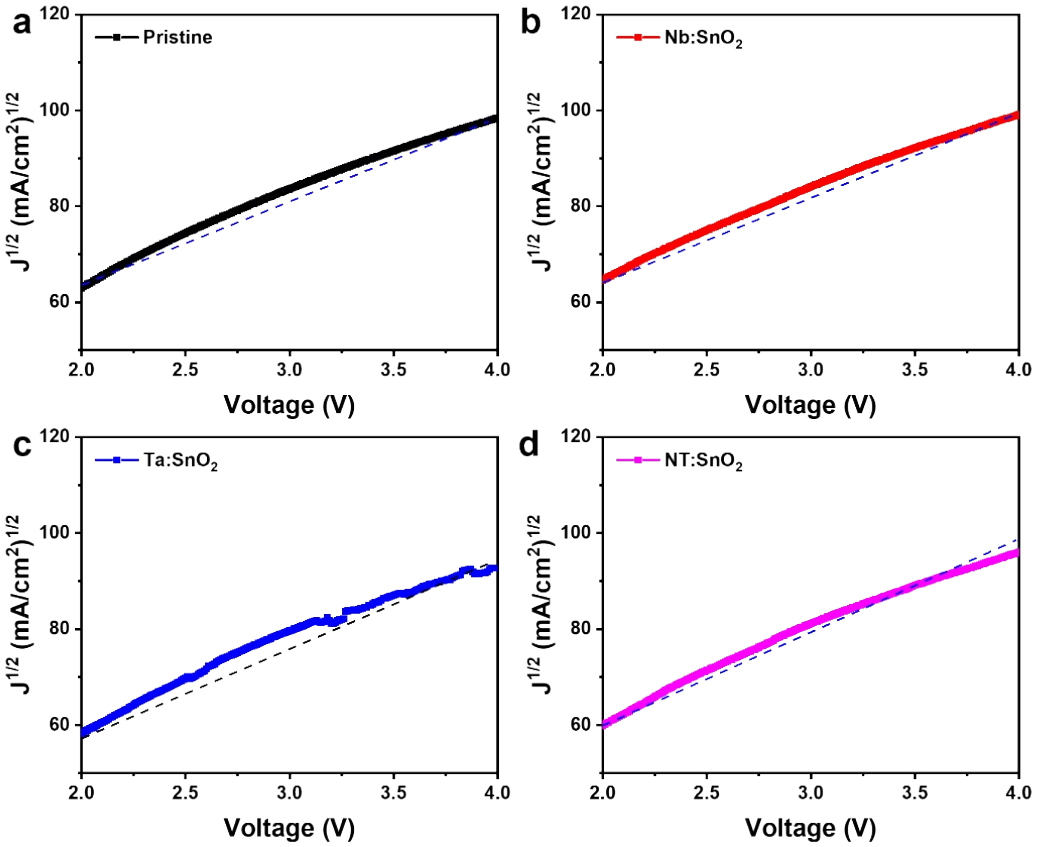

Fig. S3. Electron mobility of (a) the pristine SnO_2, (b) Nb:SnO_2, (c) Ta:SnO_2, and (d) NT:SnO_2.

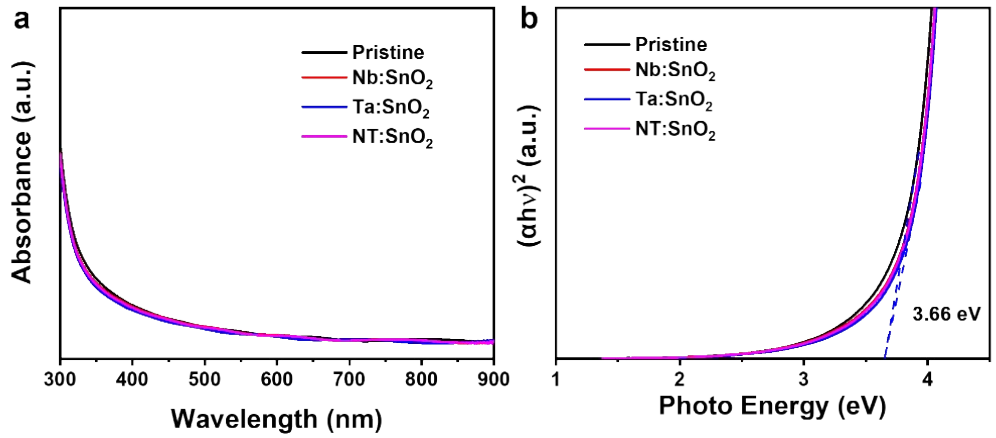

Fig. S4. (a) UV-vis absorption spectra of the pristine and doped SnO_2 films, (b) the corresponding bandgaps.

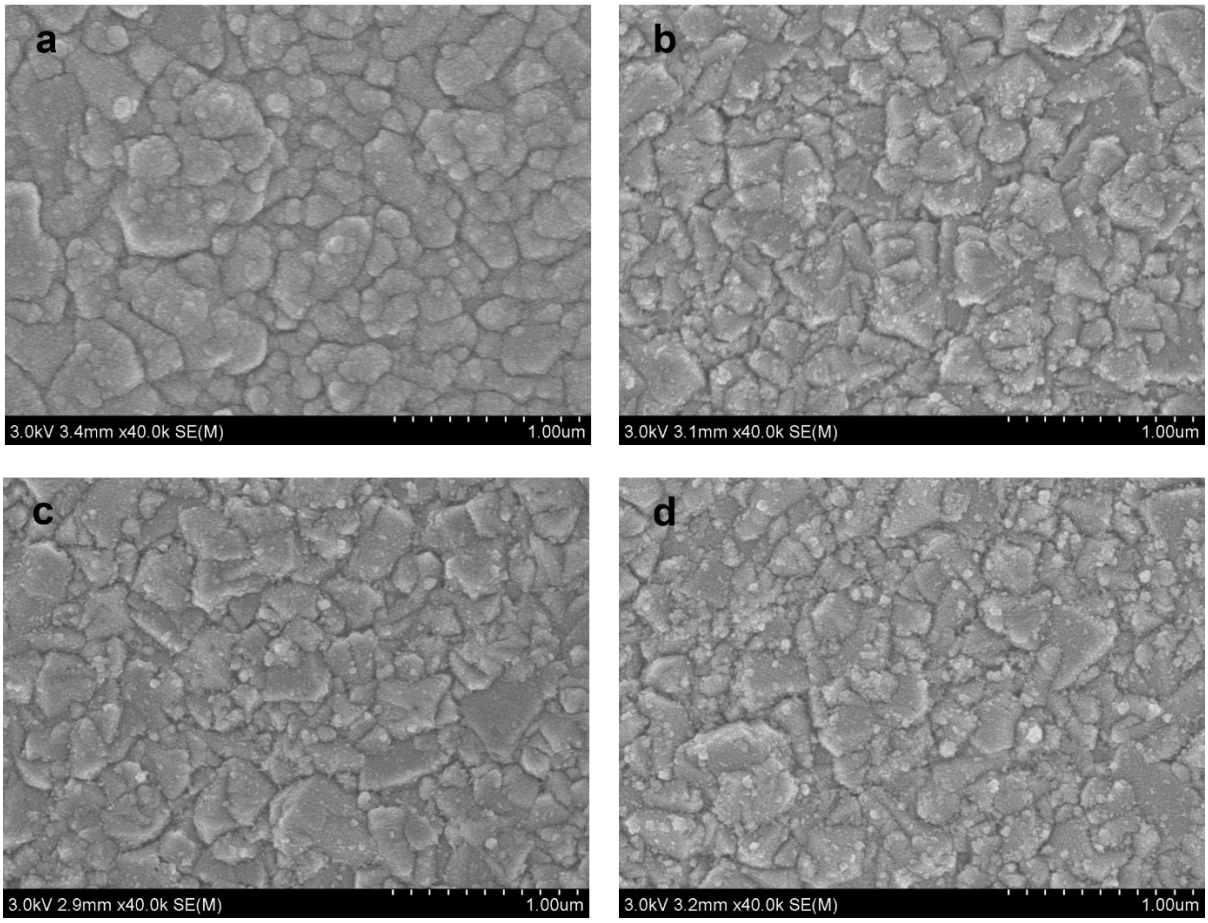

Fig. S5. SEM images of (a) the pristine SnO_2, (b) Nb:SnO_2, (c) Ta:SnO_2, and (d) NT:SnO_2 films.

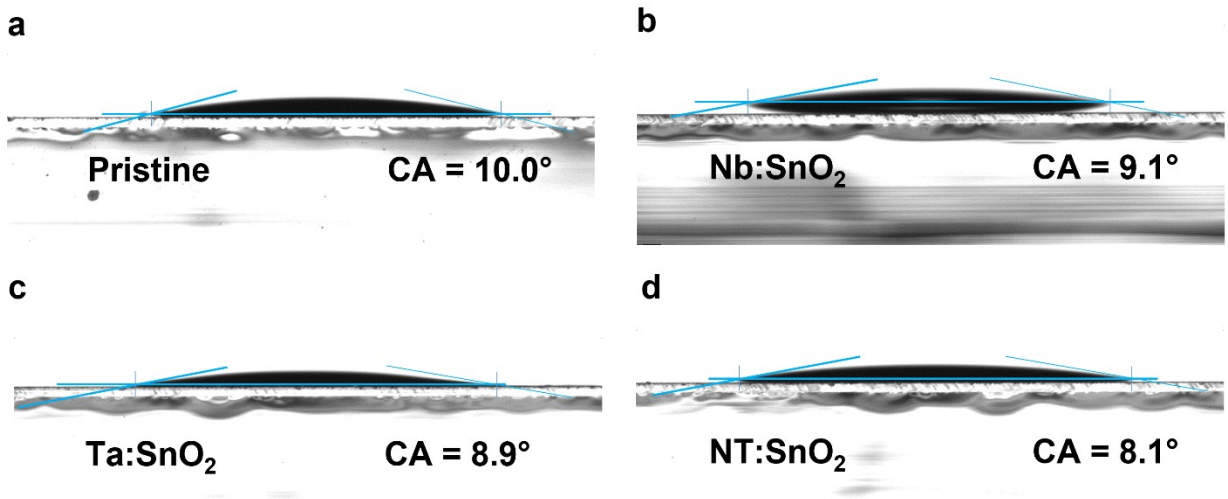

Fig. S6. Contact angles of perovskite solution based on (a) the pristine SnO_2, (b) Nb:SnO_2, (c) Ta:SnO_2, and (d) NT:SnO_2 films.

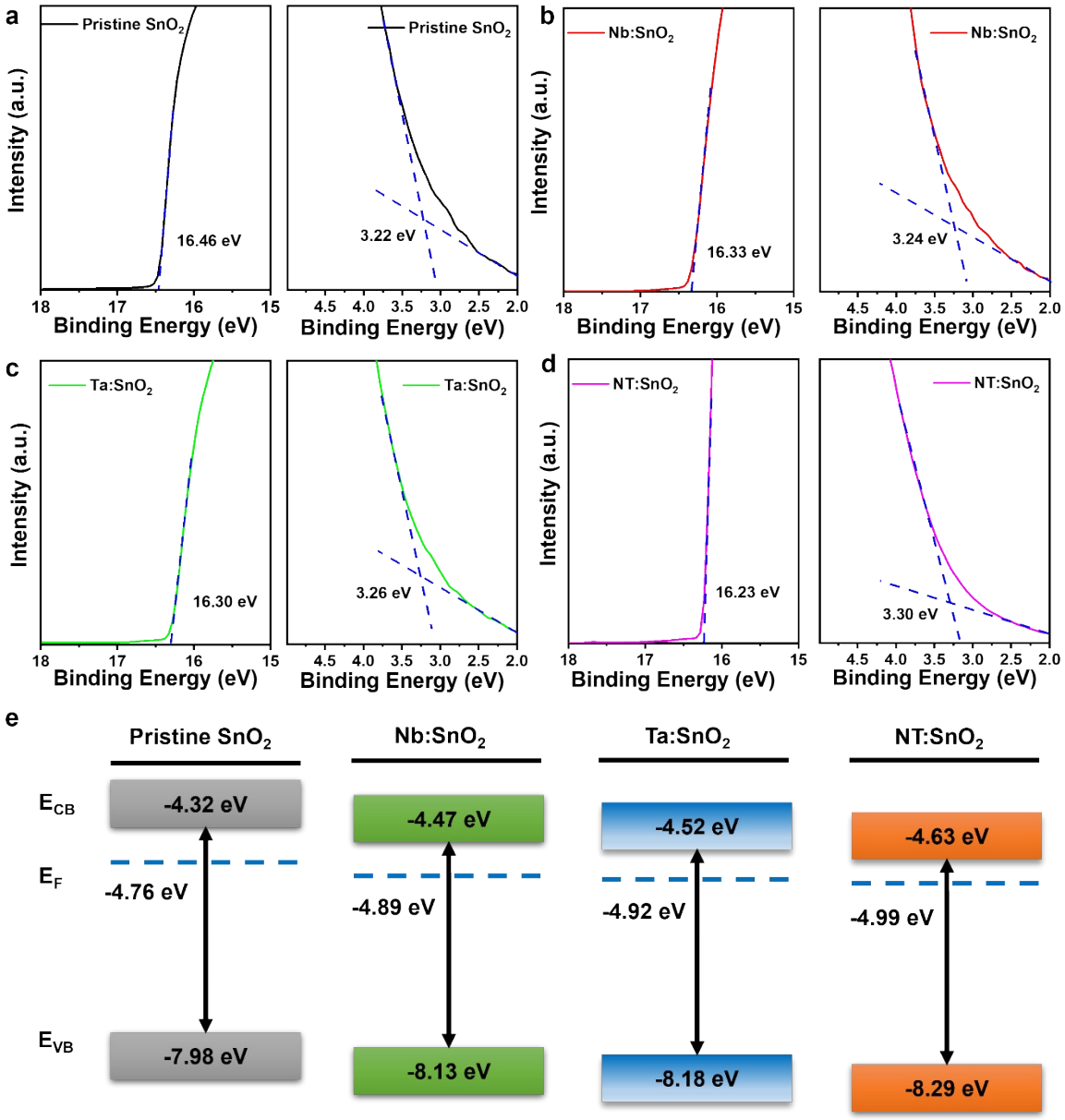

Fig. S7. UPS spectra of (a) the pristine SnO_2, (b) Nb:SnO_2, (c) Ta:SnO_2, (d) NT:SnO_2, and (e) the corresponding energy levels.

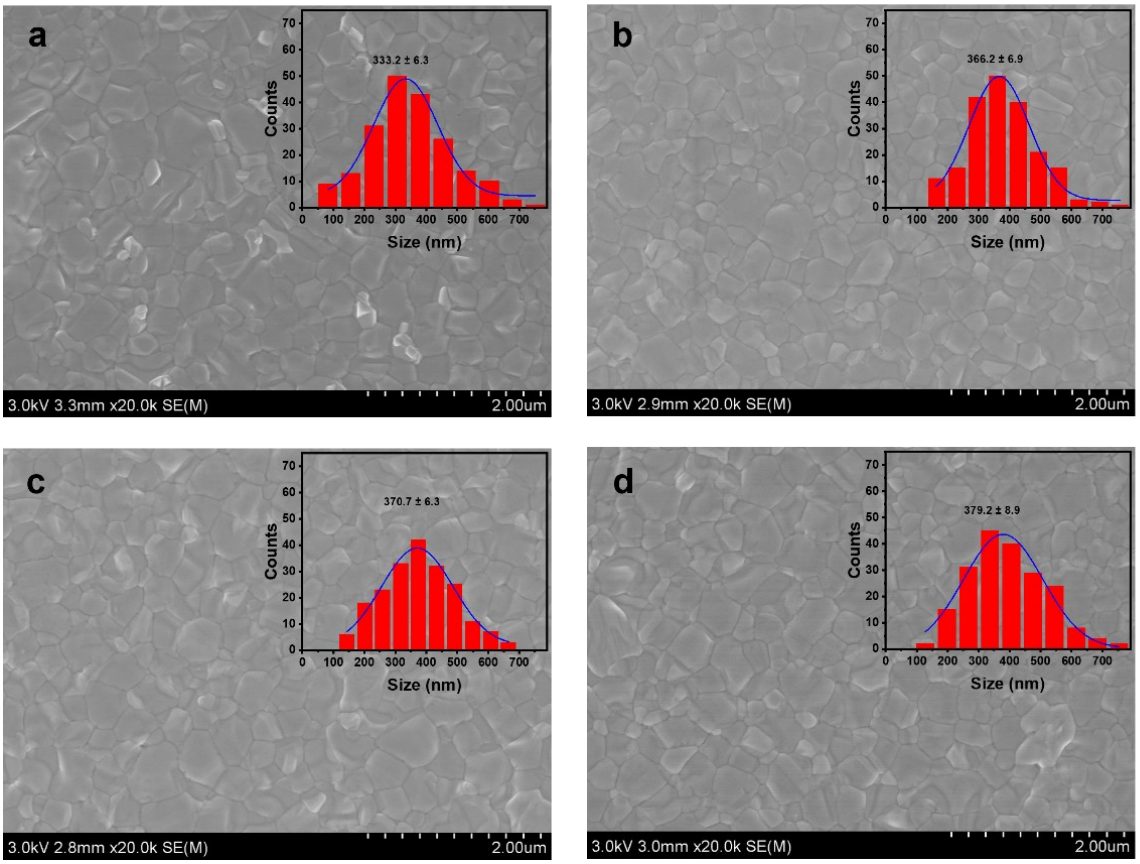

Fig. S8. SEM images and the corresponding grain size distributions of perovskite films based on (a) the pristine SnO_2, (b) Nb:SnO_2, (c) Ta:SnO_2, and (d) NT:SnO_2.

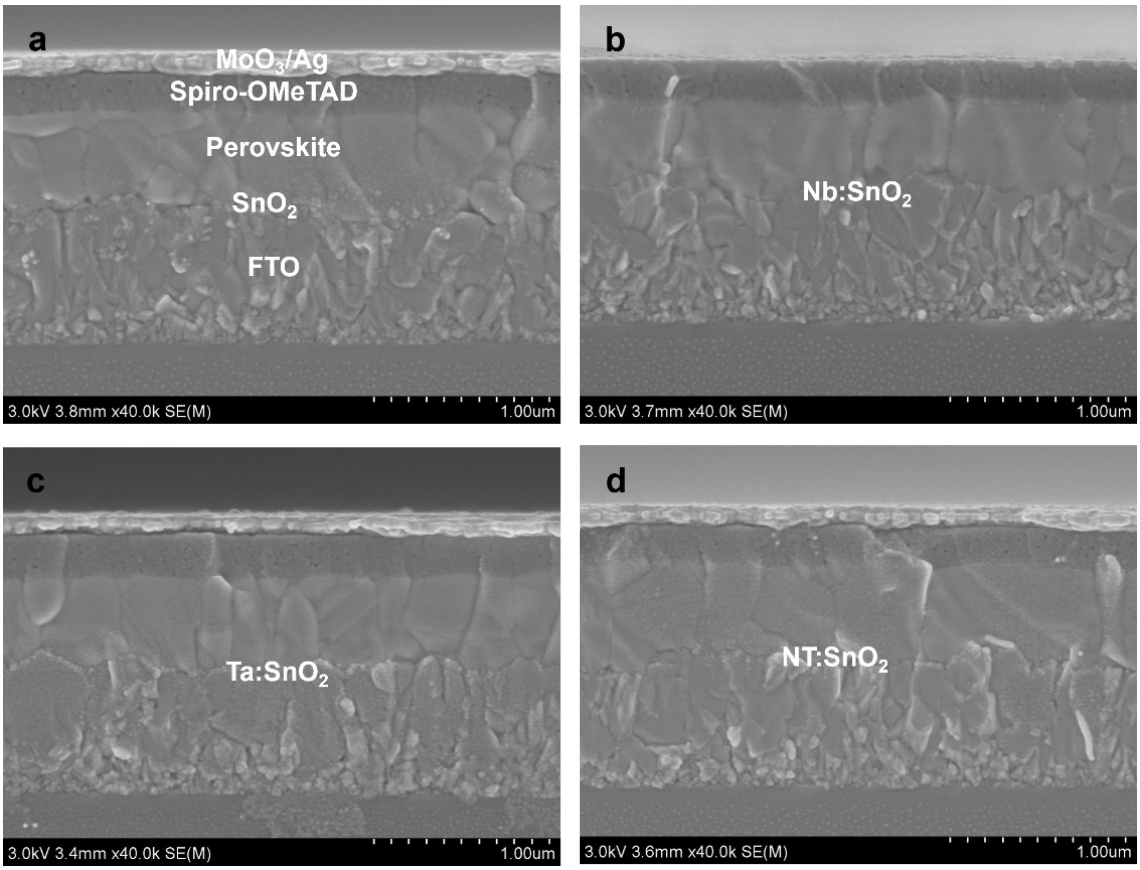

Fig. S9. Cross-sectional SEM images of the devices based on (a) the pristine SnO_2, (b) Nb:SnO_2, (c) Ta:SnO_2, and (d) NT:SnO_2.

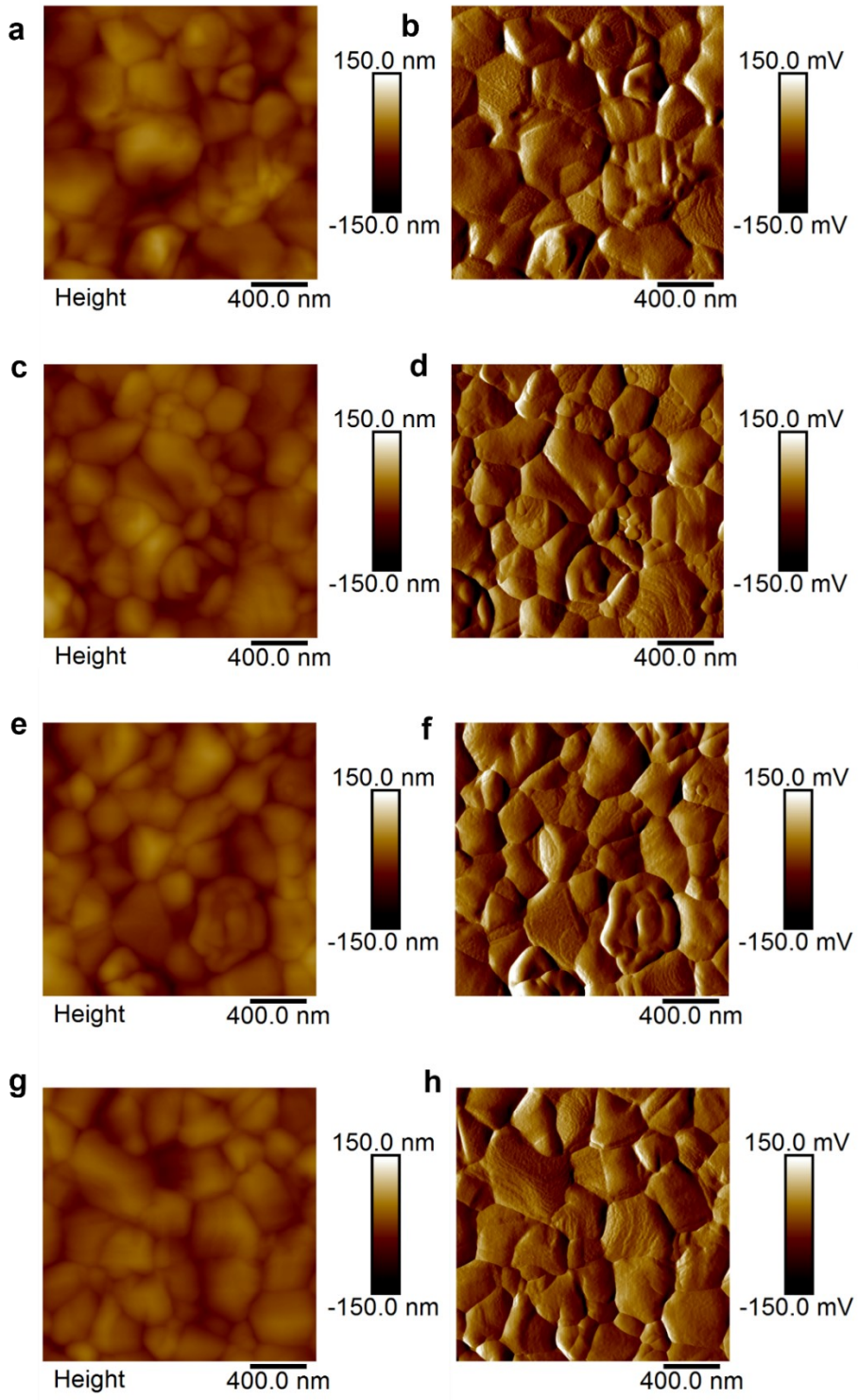

Fig. S10. AFM images and the corresponding amplitude of the perovskite films based on (a) the pristine SnO_2, (b) Nb:SnO_2, (c) Ta:SnO_2, and (d) NT:SnO_2.

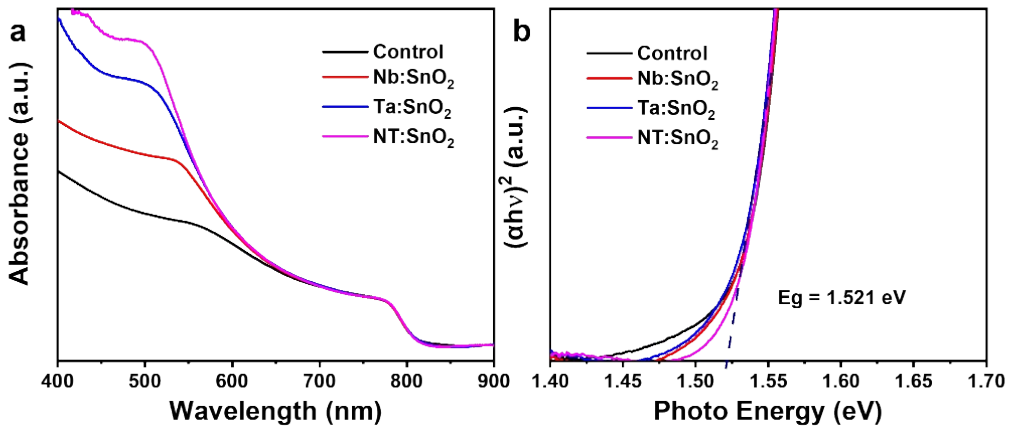

Fig. S11 (a) The UV-vis absorption spectra of the perovskite films based on the pristine and doped SnO_2 films, (b) the corresponding bandgaps.

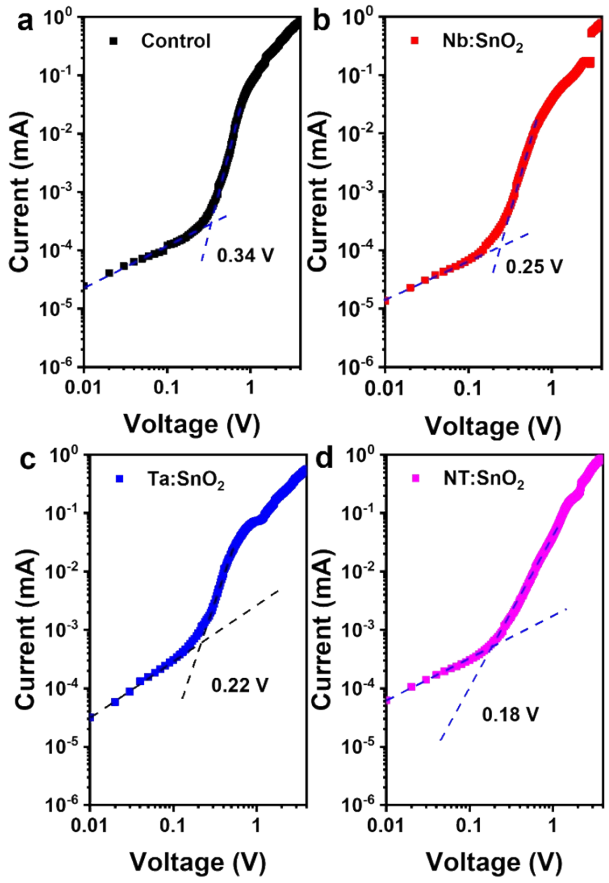

Fig. S12. Dark I-V curves for the electron-only devices based on (a) the pristine SnO_2, (b) Nb:SnO_2, (c) Ta:SnO_2, and (d) NT:SnO_2. (Device structure: FTO/SnO_2/perovskite/PCBM/Ag)

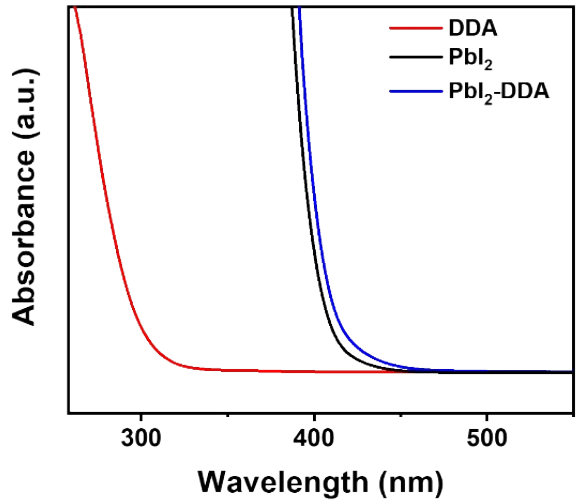

Fig. S13. UV-vis absorption spectra for DDA, PbI_2, and DDA-PbI_2 (Solvent: DMSO).

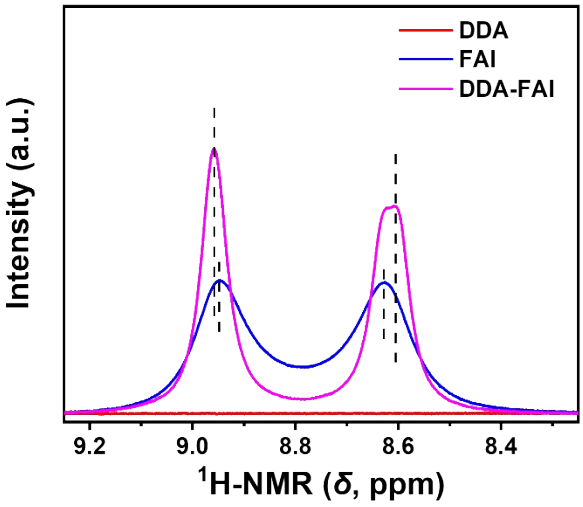

Fig. S14. The proton signal of N-H in DDA, FAI, and DDA mixed FAI samples (^{1}H NMR, DMSO-d6).

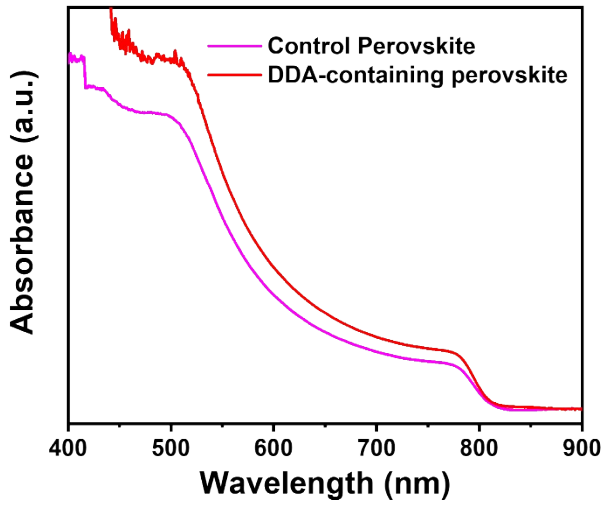

Fig. S15. UV-vis absorption spectra for the control and DDA-treated perovskite films.

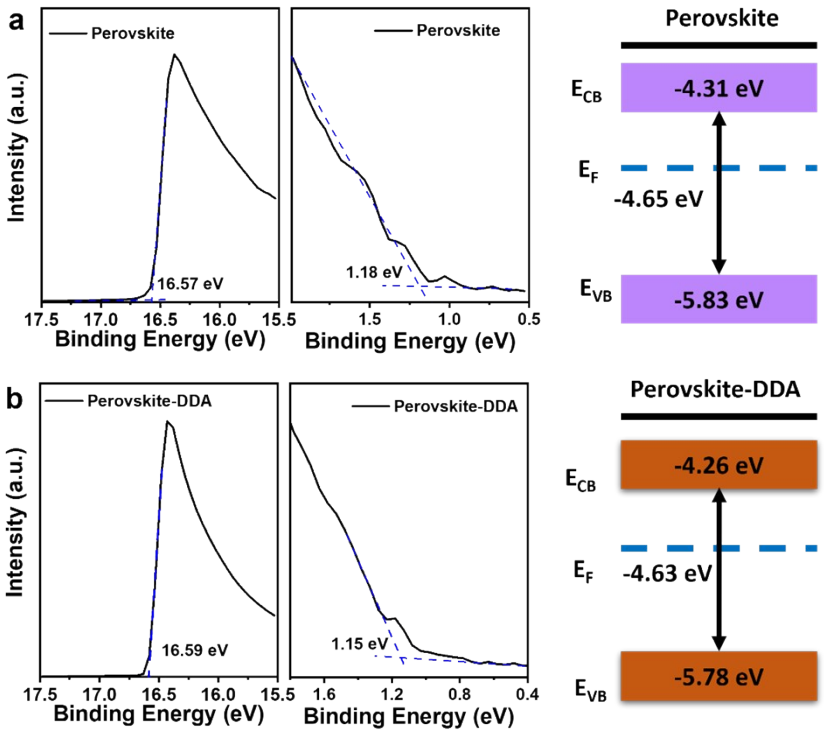

Fig. S16. UPS and energy levels for (a) perovskite and (b) perovskite with DDA treatment.

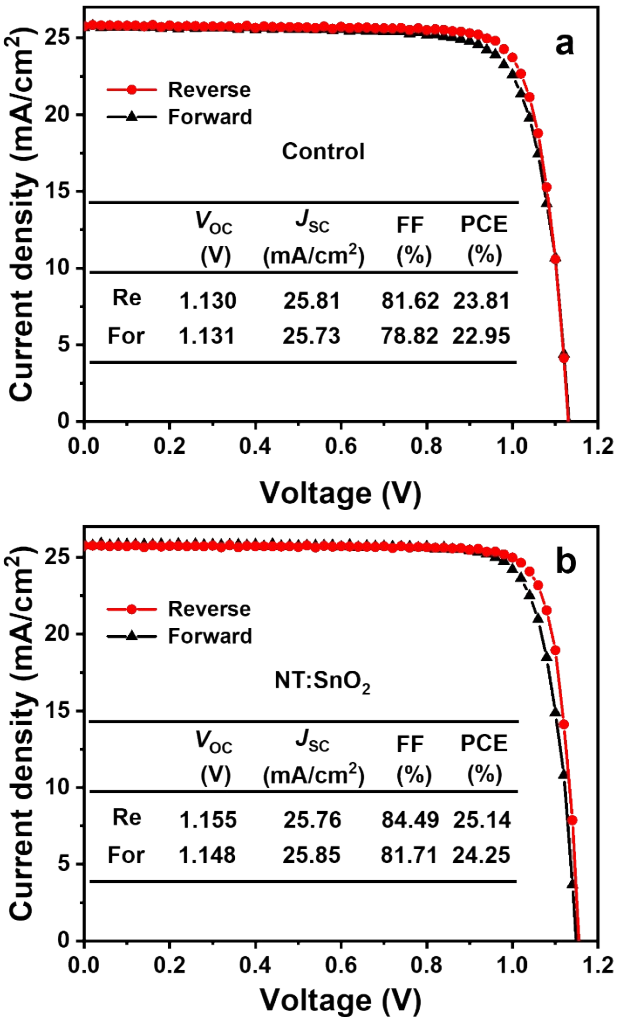

Fig. S17. The hysteresis effect of the (a) control and (b) NT:SnO_2 based devices.

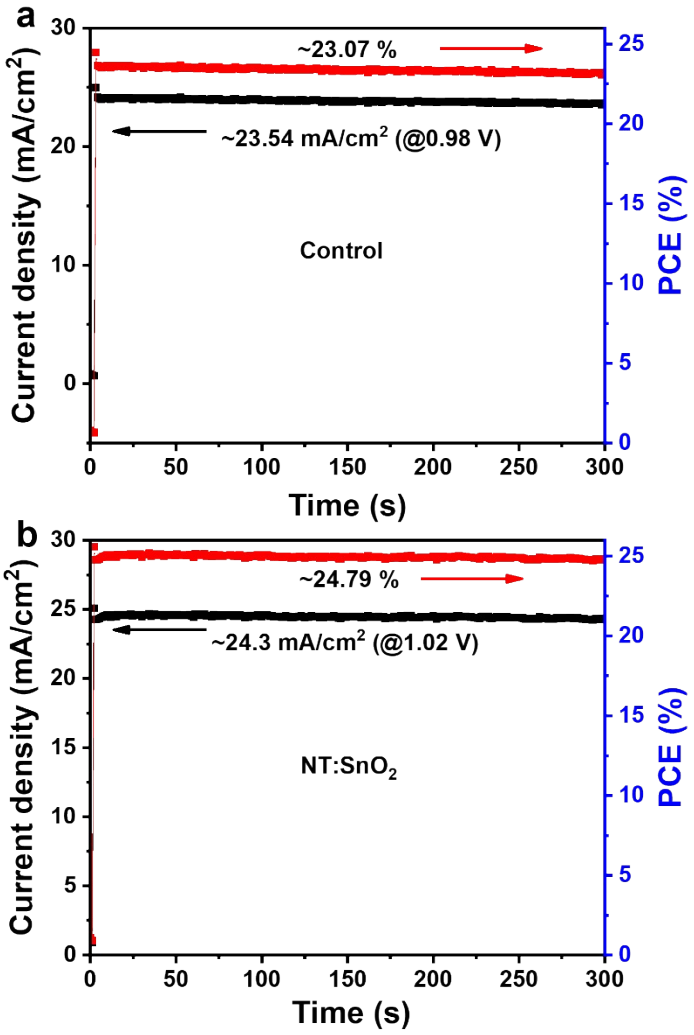

Fig. S18. Stabilized output efficiency of (a) the control and (b) NT:SnO_2 devices around the maximum output power point as a function of time under simulated 1 sun illumination.

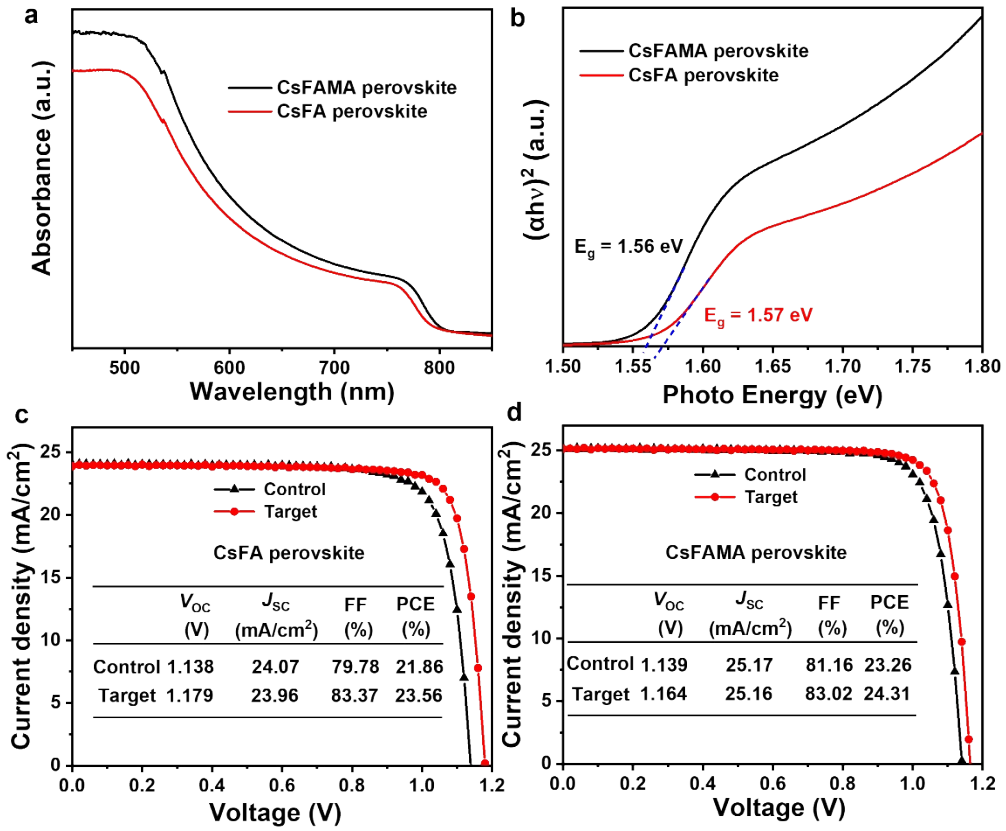

Fig. S19. (a) UV-vis absorption spectra and (b) corresponding bandgaps of CsFA and CsFAMA-based perovskites. *J-V* curves of the optimized PSCs (NT:SnO_2 + DDA treatment) based on (c) CsFA and (d) CsFAMA perovskites.

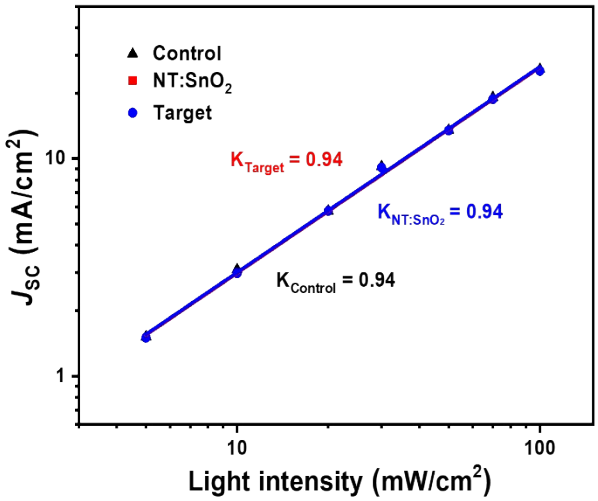

Fig. S20. J_{SC} *vs.* light intensity for the control, NT:SnO_2-based and target devices.

Table S1. Summary of PV parameters for PSCs based on RbCsFAMA quadruple cation perovskites.

Devices Configurations	Eg [eV]	Scan direction	V_{OC} [V]	J_{SC} [mA/cm^2]	FF [%]	PCE [%]	Ref.
P-I-N: ITO/PTAA/$Rb_{0.025}Cs_{0.025}FA_{0.7}MA_{0.25}PbI_3$/$CdI_2$/$C_{60}$/BCP/Cu	1.51	Reverse	1.200	23.50	77.70	21.90	1
		Forward	1.200	23.30	77.60	21.70	
P-I-N: ITO/PTAA/$Rb_{0.05}Cs_{0.05}FA_{0.85}MA_{0.05}PbI_{2.85}Br_{0.15}$/C60/BCP/Cu	N/A	Reverse	1.150	23.40	81.70	22.00	2
		Forward	/	/	/	/	
P-I-N: FTO/NiOx/$Rb_{0.2}Cs_{0.2}FA_{0.3}MA_{0.3}$/$PC_{61}BM$/BCP/Ag	1.63	Reverse	1.250	23.70	77.00	22.81	3
		Forward	/	/	/	/	
P-I-N: ITO/PTAA/$Rb_{0.05}Cs_{0.05}FA_{0.79}MA_{0.16}PbI_{1.8}Br_{1.2}$/SG/$PC_{61}BM$/BCP/Ag	1.78	Reverse	1.190	18.53	80.30	17.71	4
		Forward	1.190	18.62	79.30	17.57	
P-I-N: ITO/PTAA:BDT-Si/$Rb_{0.05}Cs_{0.05}FA_{0.8}MA_{0.1}PbI_{2.85}Br_{0.15}$/$PC_{61}BM$/BCP/Cu	1.53	Reverse	1.100	24.44	81.37	21.87	5
		Forward	/	/	/	/	
P-I-N: ITO/MeO-2PACz/$Rb_{0.05}Cs_{0.05}FA_{0.85}MA_{0.05}PbI_{2.85}Br_{0.15}$/LiF/C60/BCP/Ag	1.53	Reverse	1.150	26.13	84.60	25.49	6
		Forward	1.150	26.19	83.90	25.27	
N-I-P: FTO/c-TiO_2/m-TiO_2/$Rb_{0.05}(Cs_{0.05}FAMA)_{0.95}$/spiro-OMeTAD/Au	1.63	Reverse	1.180	22.80	81.00	21.80	7
		Forward	1.173	22.80	80.00	21.30	
N-I-P: FTO/c-TiO_2/m-TiO_2/$Rb_{0.05}(Cs_{0.05}FAMAPb)_{0.95}$ /spiro-OMeTAD/Au	1.63	Reverse	1.160	22.90	78.00	21.10	8
		Forward	/	/	/	/	
N-I-P: ITO/SnO_2/$Rb_{0.09}Cs_{0.05}FA_{0.85}MA_{0.15}PbI_{2.85}Br_{0.15}$/spiro-OMeTAD/Au	1.63	Reverse	1.160	24.00	75.89	20.85	9
		Forward	/	/	/	/	
N-I-P: FTO/SnO_2/$Rb_{0.05}Cs_{0.05}FA_{0.83}MA_{0.17}PbI_{2.85}Br_{0.15}$/spiro-OMeTAD/Ag	1.56	Reverse	1.098	24.11	80.77	21.38	10
		Forward	1.084	24.09	79.40	20.73	
N-I-P: FTO/c-TiO_2/m-TiO_2/PMMA:PCBM/$Rb_{0.03}Cs_{0.07}FA_{0.765}MA_{0.135}PbI_{2.55}Br_{0.45}$/spiro-OMeTAD/Au	1.60	Reverse	1.200	23.94	79.31	22.77	11
		Forward	1.200	23.97	78.56	22.59	
N-I-P: ITO/c-TiO_2/m-TiO_2/$Rb_{0.05}Cs_{0.095}FA_{0.7125}MA_{0.1425}PbI_2Br$/spiro-OMeTAD/Au	1.72	Reverse	1.269	18.90	76.20	18.30	12
		Forward	1.265	18.90	76.50	18.30	
N-I-P: FTO/c-TiO_2/m-TiO_2/RbCsFAMA/Spiro-	N/A	Reverse	1.161	22.28	76.80	20.24	13

OMeTAD/Au		Forward	1.161	22.27	75.90	20.03	
N-I-P: FTO/c-TiO_2/m-TiO_2/$Rb_{0.06}Cs_{0.08}FA_{0.78}MA_{0.08}PbI_{2.76}Br_{0.24}$/Spiro-OMeTAD/Au	1.55	Reverse	1.162	24.75	76.00	22.18	14
		Forward	1.151	24.72	75.70	21.70	
N-I-P: ITO/SnO_2/$Rb_{0.05}Cs_{0.05}(FA_{0.83}MA_{0.17})_{0.9}PbI_{2.49}Br_{5.1}$/spiro-OMeTAD/Au	1.63	Reverse	1.240	22.37	77.65	21.54	15
		Forward	1.239	22.37	77.52	21.49	
N-I-P: FTO/TiO_2/m-TiO_2/$Rb_{0.03}Cs_{0.05}FA_{0.90}MA_{0.05}PbI_3$/spiro-OMeTAD/Au.	1.54	Reverse	1.121	25.35	84.70	24.05	16
		Forward	1.123	25.23	80.50	22.85	
N-I-P: FTO/SnO_2/$Rb_{0.03}Cs_{0.05}FA_{0.90}MA_{0.05}PbI_3$/spiro-OMeTAD/$MoO_3$/Ag	1.52	Reverse	1.159	25.51	83.56	24.71	17
		Forward	1.147	25.66	81.27	23.92	
N-I-P: FTO/SnO_2/$Rb_{0.03}Cs_{0.05}FA_{0.90}MA_{0.05}PbI_3$/spiro-OMeTAD/$MoO_3$/Ag	1.52	Reverse	1.162	25.69	83.80	25.01	18
		Forward	1.146	25.65	80.78	23.74	
N-I-P: FTO/SnO_2/$Rb_{0.03}Cs_{0.05}FA_{0.90}MA_{0.05}PbI_3$/spiro-OMeTAD/$MoO_3$/Ag	1.52	Reverse	1.160	25.80	84.51	25.30	**This work**
		Forward	1.154	25.75	82.71	24.58	

Table S2. Parameters of the TRPL spectroscopy based on different samples.

Samples	τ_{ave} (ns)	τ_1 (ns)	τ_2 (ns)	A_1	A_2
Glass/perovskite	2700.0	13.1	2736.8	0.13	0.78
Glass/perovskite-DDA	3511.8	17.6	3520.8	0.30	0.58

Table S3. EIS parameters of the control, NT:SnO_2 and target devices.

Devices	R_{tr} (Ω)	CPE1 (F)	R_{rec} (Ω)	CPE2 (F)
Control	14820	9.64E-09	8.10E+04	3.47E-07
NT:SnO_2	13475	1.09E-08	1.49E+05	1.10E-06
Target	11693	1.15E-08	1.69E+05	8.50E-07

Table S4. Time evolution of the PV parameters for the control and target PSCs.

Devices	Time (h)	V_{OC} (V)	J_{SC} (mA cm^{-2})	FF (%)	PCE (%)
Control	0	1.13	25.81	81.62	23.81
	24	1.13	25.53	82.23	23.67
	48	1.13	25.45	81.48	23.33
	72	1.11	25.38	81.22	22.78
	120	1.11	25.33	79.62	22.45
	288	1.12	25.12	79.32	22.22
	456	1.10	25.21	79.21	22.05
	672	1.08	24.80	75.20	20.05
	912	1.07	24.73	74.17	19.59
	1176	1.07	24.81	72.43	19.17
	1512	1.03	24.50	69.26	17.48
	1896	1.03	23.33	61.76	14.86
Target	0	1.16	25.83	83.44	24.96
	24	1.17	25.66	83.55	25.00
	48	1.16	25.75	83.64	24.92
	72	1.16	25.71	83.25	24.89
	120	1.15	25.76	83.39	24.81
	288	1.15	25.70	83.82	24.74
	456	1.15	25.49	83.48	24.57
	672	1.14	25.52	83.13	24.27
	912	1.14	25.51	82.30	23.86
	1176	1.13	25.46	80.20	23.15
	1512	1.13	25.33	79.94	22.81
	1896	1.12	25.36	78.84	22.42
	2304	1.12	25.28	78.82	22.31
	2612	1.11	25.34	78.58	22.19

References:

1. W.-Q. Wu, P. N. Rudd, Z. Ni, C. H. Van Brackle, H. Wei, Q. Wang, B. R. Ecker, Y. Gao and J. Huang, *J. Am. Chem. Soc.*, 2020, **142**, 3989-3996.
2. S. Chen, Y. Liu, X. Xiao, Z. Yu, Y. Deng, X. Dai, Z. Ni and J. Huang, *Joule*, 2020, **4**, 2661-2674.
3. B. Gao and J. Meng, *Appl Surf Sci*, 2020, **530**, 147240.
4. K. M. Reza, A. Gurung, B. Bahrami, A. H. Chowdhury, N. Ghimire, R. Pathak, S. I. Rahman, M. A. R. Laskar, K. Chen, R. S. Bobba, B. S. Lamsal, L. K. Biswas, Y. Zhou, B. Logue and Q. Qiao, *Solar RRL*, 2021, **5**, 2000740.
5. G. Xu, R. Xue, S. J. Stuard, H. Ade, C. Zhang, J. Yao, Y. Li and Y. Li, *Adv. Mater.*, 2021, **33**, 2006753.
6. Q. Jiang, J. Tong, Y. Xian, R. A. Kerner, S. P. Dunfield, C. Xiao, R. A. Scheidt, D. Kuciauskas, X. Wang, M. P. Hautzinger, R. Tirawat, M. C. Beard, D. P. Fenning, J. J. Berry, B. W. Larson, Y. Yan and K. Zhu, *Nature*, 2022, **611**, 278-283.
7. M. Saliba, T. Matsui, K. Domanski, J.-Y. Seo, A. Ummadisingu, S. M. Zakeeruddin, J.-P. Correa-Baena, W. R. Tress, A. Abate, A. Hagfeldt and M. Grätzel, *Science*, 2016, **354**, 206-209.
8. P. Yadav, M. I. Dar, N. Arora, E. A. Alharbi, F. Giordano, S. M. Zakeeruddin and M. Grätzel, *Adv. Mater.*, 2017, **29**, 1701077.
9. S. Ma, Y. Bai, H. Wang, H. Zai, J. Wu, L. Li, S. Xiang, N. Liu, L. Liu, C. Zhu, G. Liu, X. Niu, H. Chen, H. Zhou, Y. Li and Q. Chen, *Adv. Energy Mater.*, 2020, **10**, 1902472.
10. L. Yangi, Y. Li, Y. Pei, J. Wang, H. Lin and X. Li, *J. Mater. Chem. A*, 2020, **8**, 7808-7818.
11. M. A. Mahmud, T. Duong, Y. Yin, H. T. Pham, D. Walter, J. Peng, Y. Wu, L. Li, H. Shen, N. Wu, N. Mozaffari, G. Andersson, K. R. Catchpole, K. J. Weber and T. P. White, *Adv. Funct. Mater.*, 2020, **30**, 1907962.
12. T. Duong, H. Pham, T. C. Kho, P. Phang, K. C. Fong, D. Yan, Y. Yin, J. Peng, M. A. Mahmud, S. Gharibzadeh, B. A. Nejand, I. M. Hossain, M. R. Khan, N. Mozaffari, Y. Wu, H. Shen, J. Zheng, H. Mai, W. Liang, C. Samundsett, M. Stocks, K. McIntosh, G. G. Andersson, U. Lemmer, B. S. Richards, U. W. Paetzold, A. Ho-Ballie, Y. Liu, D. Macdonald, A. Blakers, J. Wong-Leung, T. White, K. Weber and K. Catchpole, *Adv. Energy Mater.*, 2020, **10**, 1903553.
13. L. Merten, A. Hinderhofer, T. Baumeler, N. Arora, J. Hagenlocher, S. M. Zakeeruddin, M. I. Dar, M. Grätzel and F. Schreiber, *Chem. Mater.*, 2021, **33**, 2769-2776.
14. E. A. Alharbi, T. P. Baumeler, A. Krishna, A. Y. Alyamani, F. T. Eickemeyer, O. Ouellette, L. Pan, F. S. Alghamdi, Z. Wang, M. H. Alotaibi, B. Yang, M. Almalki, M. D. Mensi, H. Albrithen, A. Albadri, A. Hagfeldt, S. M. Zakeeruddin and M. Grätzel, *Adv. Energy Mater.*, 2021, **11**, 2003785.
15. G. Yang, Z. Ren, K. Liu, M. Qin, W. Deng, H. Zhang, H. Wang, J. Liang, F. Ye, Q. Liang, H. Yin, Y. Chen, Y. Zhuang, S. Li, B. Gao, J. Wang, T. Shi, X. Wang, X. Lu, H. Wu, J. Hou, D. Lei, S. K. So, Y.

Yang, G. Fang and G. Li, *Nat. Photonics*, 2021, **15**, 681-689.

16. Y. Ding, B. Ding, H. Kanda, O. J. Usiobo, T. Gallet, Z. Yang, Y. Liu, H. Huang, J. Sheng, C. Liu, Y. Yang, V. I. E. Queloz, X. Zhang, J.-N. Audinot, A. Redinger, W. Dang, E. Mosconic, W. Luo, F. De Angelis, M. Wang, P. Dörflinger, M. Armer, V. Schmid, R. Wang, K. G. Brooks, J. Wu, V. Dyakonov, G. Yang, S. Dai, P. J. Dyson and M. K. Nazeeruddin, *Nat. Nanotech.*, 2022, **17**, 598-605.
17. Y. Chen, Q. Wang, W. Tang, W. Qiu, Y. Wu and Q. Peng, *Nano Energy*, 2023, **107**, 108154.
18. Q. Wang, W. Tang, Y. Chen, W. Qiu, Y. Wu and Q. Peng, *J. Mater. Chem. A*, 2023, **11**, 1170-1179.